Misaligned Antenna Phase-Center Determination Using Measured Phase Patterns

A. Prata, Jr.[1]

When an antenna is first mounted on a test range and its radiation pattern measured, invariably one finds that the antenna is improperly aligned. In other words, the test positioner is not rotating about the antenna phase center (defined in some appropriate sense). Since for a variety of reasons it is desirable to measure the antenna by rotating about its phase center, a procedure is needed for its location. In this article, a method for locating the phase center of an antenna, from phase patterns measured on a misaligned antenna, is presented.

I. Phase Error of a Misaligned Antenna

Consider Figs. 1 and 2 depicting the location of the phase center of the antenna under test (AUT), the illuminating antenna phase-center location, and three relevant coordinate systems, which relate to each other through the equations

$$\hat{x}_P = \hat{x}_F \cos\phi - \hat{y}_F \sin\phi \tag{1}$$

$$\hat{y}_P = \hat{x}_F \sin\phi + \hat{y}_F \cos\phi \tag{2}$$

$$\hat{z}_P = \hat{z}_F \tag{3}$$

and

$$\hat{x} = \hat{x}_P \tag{4}$$

$$\hat{y} = \hat{y}_P \cos\theta - \hat{z}_P \sin\theta \tag{5}$$

$$\hat{z} = \hat{y}_P \sin\theta + \hat{z}_P \cos\theta \tag{6}$$

where the hats denote unit vectors.

[1] Department of Electrical Engineering—Electrophysics, University of Southern California, Los Angeles, and Spacecraft Telecommunications Equipment Section.

The research described in this publication was carried out by the Jet Propulsion Laboratory, California Institute of Technology, under a contract with the National Aeronautics and Space Administration.

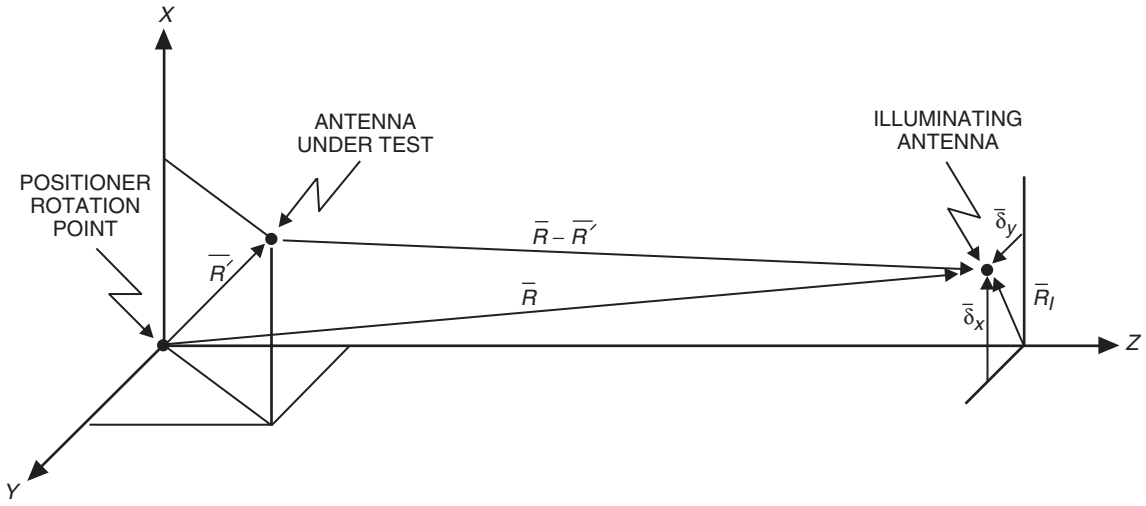

Fig. 1. Radiation-pattern measurement geometry.

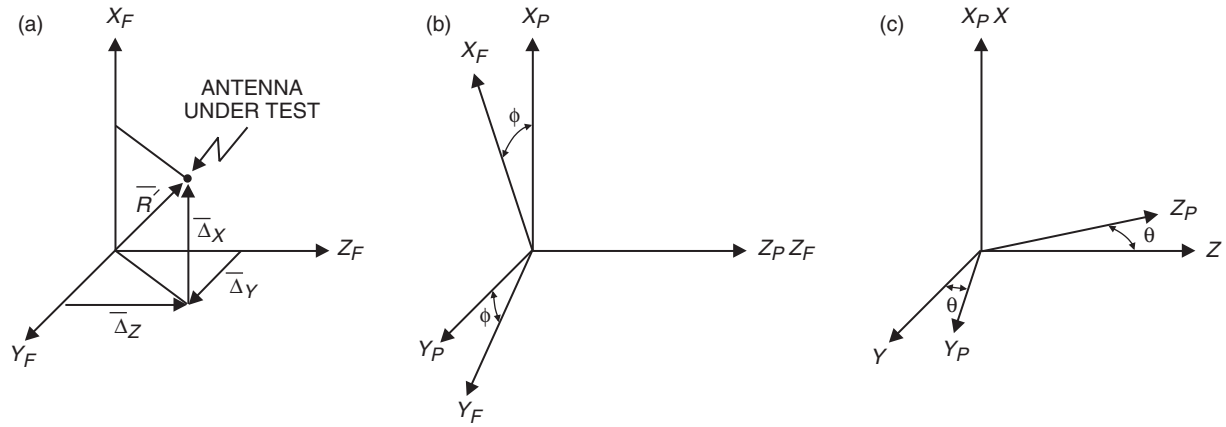

Fig. 2. Relevant coordinate systems of the radiation-pattern measurement geometry and associated movements: (a) antenna-under-test displacement, (b) test positioner axial rotation, and (c) test positioner azimuthal rotation.

The AUT is mounted on a test positioner with axial rotation (i.e., ϕ) and azimuth (i.e., θ) orientation capabilities. In an experimental setup the principal coordinate system direction $\hat{x}$ is usually perpendicular to the ground. The illuminating antenna is located near the z-axis, at a distance R from the three coordinate systems' origin. Note that the particular geometry that should be considered in an analysis depends both on the measurement setup and on how the AUT is mounted. Here only the measurement setup just described is being considered.

The AUT radiation pattern is measured by incrementing the spherical angle θ (with a constant ϕ value) while the complex signal received by the AUT is recorded. As depicted in Fig. 2, misalignment causes the phase center of the AUT to be displaced by a small vector

$$\vec{R}' = \vec{\Delta}_x + \vec{\Delta}_y + \vec{\Delta}_z \tag{7}$$

from the positioner rotation point (PRP). Furthermore, the illuminating antenna misalignment also causes its phase center to be displaced from the z-axis by a small vector $\vec{R}_I$:

$$\vec{R}_I = \vec{\delta}_x + \vec{\delta}_y \tag{8}$$

Since the AUT phase center is not properly aligned with the PRP, and the illuminating antenna is not along the z-axis, when the AUT pattern is measured a spurious phase error will be produced. Assuming an implicit $e^{j\omega t}$ time-harmonic regimen, the measured AUT phase pattern $\Phi(\theta, \phi)$ is given by

$$\Phi(\theta, \phi) = -k_0 |\vec{R} - \vec{R}'| + F(\theta, \phi) \tag{9}$$

where k_0 is the free-space wave number ($k_0 = 2\pi/\lambda_0$, where λ_0 is the free-space wavelength), and $F(\theta, \phi)$ is the phase pattern of the AUT when its phase center coincides with the PRP. Using Eqs. (7) and (8), one has from Figs. 1 and 2

$$\vec{R} - \vec{R}' = \delta_x \, \hat{x} + + \delta_y \, \hat{y} + R \, \hat{z} - \Delta_x \, \hat{x}_F - \Delta_y \, \hat{y}_F - \Delta_z \, \hat{z}_F \tag{10}$$

which yields

$$\begin{aligned} \left| \vec{R} - \vec{R}' \right| = \big[& (+\delta_x \hat{x} + \delta_y \hat{y} + R\hat{z} - \Delta_x \hat{x}_F - \Delta_y \hat{y}_F - \Delta_z \hat{z}_F) \\ & \cdot (+\delta_x \hat{x} + \delta_y \hat{y} + R\hat{z} - \Delta_x \hat{x}_F - \Delta_y \, \hat{y}_F - \Delta_z \hat{z}_F) \big]^{1/2} \end{aligned} \tag{11}$$

Now, from Eqs. (1) through (6), one has

$$\hat{x} = \hat{x}_F \cos\phi - \hat{y}_F \sin\phi \tag{12}$$

$$\hat{y} = \hat{x}_F \sin\phi \cos\theta + \hat{y}_F \cos\phi \cos\theta - \hat{z}_F \sin\theta \tag{13}$$

$$\hat{z} = \hat{x}_F \sin\phi \sin\theta + \hat{y}_F \cos\phi \sin\theta + \hat{z}_F \cos\theta \tag{14}$$

and, hence, Eq. (11) becomes

$$\begin{aligned} \left| \vec{R} - \vec{R}' \right| = \big[& R^2 + 2R \sin\phi \sin\theta \, (\delta_x \cos\phi + \delta_y \sin\phi \cos\theta - \Delta_x) \\ & + 2R \cos\phi \sin\theta \, (-\delta_x \sin\phi + \delta_y \cos\phi \cos\theta - \Delta_y) + 2R \cos\theta \, (-\delta_y \sin\theta - \Delta_z) \\ & + (\delta_x \cos\phi + \delta_y \sin\phi \cos\theta - \Delta_x)^2 + (-\delta_x \sin\phi + \delta_y \cos\phi \cos\theta - \Delta_y)^2 \\ & + (-\delta_y \sin\theta - \Delta_z)^2 \big]^{1/2} \end{aligned} \tag{15}$$

This equation can be rewritten as

$$\left|\vec{R}-\vec{R}'\right| = R\left[1-2\frac{\Delta_x\sin\phi\sin\theta+\Delta_y\cos\phi\sin\theta+\Delta_z\cos\theta}{R}\right.$$

$$+\frac{(\delta_x\cos\phi+\delta_y\sin\phi\cos\theta-\Delta_x)^2}{R^2}+\frac{(-\delta_x\sin\phi+\delta_y\cos\phi\cos\theta-\Delta_y)^2}{R^2}$$

$$\left.+\frac{(-\delta_y\sin\theta-\Delta_z)^2}{R^2}\right]^{1/2} \tag{16}$$

Since in practice $\Delta_x, \Delta_y, \Delta_z, \delta_x, \delta_y << R$, the above expression approximates to[2]

$$\left|\vec{R}-\vec{R}'\right| \approx R-\Delta_x\sin\phi\sin\theta-\Delta_y\cos\phi\sin\theta-\Delta_z\cos\theta \tag{17}$$

Observe that the δ_x and δ_y of Eq. (16) have R^2 factors in their denominator and hence are not present in Eq. (17); they are then insignificant. Substituting the above result in Eq. (9) then yields

$$\Phi(\theta,\phi) \approx -k_0\left[R-\Delta_x\sin\phi\sin\theta-\Delta_y\cos\phi\sin\theta-\Delta_z\cos\theta\right]+F(\theta,\phi) \tag{18}$$

This equation shows that the measured phase $\Phi(\theta,\phi)$ is sensitive only to the phase-center displacements that occur in the measurement plane. In other words, when $\phi = 0$ deg, the measured phase $\Phi(\theta, 0 \text{ deg})$ is sensitive only to Δ_y and Δ_z, and when $\phi = 90$ deg the measured phase $\Phi(\theta, 90 \text{ deg})$ is sensitive only to Δ_x and Δ_z. This fact will be used in the next section to determine the Δ_x, Δ_y, and Δ_z values from measured phase patterns.

II. Phase-Center Determination

If the AUT were a perfect spherical-wave source, one would obtain a phase pattern [given by Eq. (18)] with a θ and ϕ independent $F(\theta,\phi)$. Introducing then a constant $C = -k_0R + F(\theta,\phi)$, one can write, for a perfect spherical wave source,

$$\Phi(\theta,\phi) \approx k_0(\Delta_x\sin\phi\sin\theta+\Delta_y\cos\phi\sin\theta+\Delta_z\cos\theta)+C \tag{19}$$

However, since the AUT does not radiate a perfect spherical wave, in general the above equation can be expected to hold for only four spatial directions (since the equation has only four degrees of freedom, namely Δ_x, Δ_y, Δ_z, and C).

Now let's assume that phase pattern measurements are made at $\phi = 0$ deg and $\phi = 90$ deg. In these two situations, the above equation becomes

$$\Phi(\theta) \approx k_0(\Delta_t\sin\theta+\Delta_z\cos\theta)+C \tag{20}$$

where Δ_t corresponds to Δ_y or Δ_x, for $\phi = 0$ deg or $\phi = 90$ deg, respectively. Since this equation has three degrees of freedom, it can be enforced at three pattern points to yield

[2] This approximation is excellent even in the improbable situation where $u = 2\Delta_{x,y,z}/R$ is comparable to 1. For instance, when $u = 0.4$, the error incurred in $\sqrt{1+u} \approx 1+u/2$ is only 1.4 percent.

$$\Phi_1 = k_0(\Delta_t \sin\theta_1 + \Delta_z \cos\theta_1) + C \tag{21}$$

$$\Phi_2 = k_0(\Delta_t \sin\theta_2 + \Delta_z \cos\theta_2) + C \tag{22}$$

$$\Phi_3 = k_0(\Delta_t \sin\theta_3 + \Delta_z \cos\theta_3) + C \tag{23}$$

where Φ_1, Φ_2, and Φ_3 are measured phase values (in radians) at the angular positions θ_1, θ_2, and θ_3, respectively.

This system can be solved for Δ_t, Δ_z, and C. To accomplish this, the value of C given by Eq. (22), namely

$$C = \Phi_2 - k_0\left(\Delta_t \sin\theta_2 + \Delta_z \cos\theta_2\right) \tag{24}$$

is substituted in Eqs. (21) and (23) to yield

$$\Phi_2 - \Phi_1 = k_0\big[\Delta_t\left(\sin\theta_2 - \sin\theta_1\right) + \Delta_z\left(\cos\theta_2 - \cos\theta_1\right)\big] \tag{25}$$

$$\Phi_2 - \Phi_3 = k_0\big[\Delta_t\left(\sin\theta_2 - \sin\theta_3\right) + \Delta_z\left(\cos\theta_2 - \cos\theta_3\right)\big] \tag{26}$$

Solving this pair of equations yields the desired Δ_t and Δ_z as

$$\Delta_z = \frac{1}{k_0}\frac{(\Phi_2 - \Phi_3)(\sin\theta_2 - \sin\theta_1) - (\Phi_2 - \Phi_1)(\sin\theta_2 - \sin\theta_3)}{(\cos\theta_2 - \cos\theta_3)(\sin\theta_2 - \sin\theta_1) - (\cos\theta_2 - \cos\theta_1)(\sin\theta_2 - \sin\theta_3)} \tag{27}$$

$$\Delta_t = \frac{1}{k_0}\frac{(\Phi_2 - \Phi_1)(\cos\theta_2 - \cos\theta_3) - (\Phi_2 - \Phi_3)(\cos\theta_2 - \cos\theta_1)}{(\cos\theta_2 - \cos\theta_3)(\sin\theta_2 - \sin\theta_1) - (\cos\theta_2 - \cos\theta_1)(\sin\theta_2 - \sin\theta_3)} \tag{28}$$

In summary, from a constant ϕ value radiation pattern phase measurement towards three directions [i.e., Φ_1, Φ_2, and Φ_3, towards (θ_1, ϕ), (θ_2, ϕ), and (θ_3, ϕ), respectively], the phase constant C, the axial phase-center displacement Δ_z, and the lateral phase-center displacement Δ_t (in the measurement plane) can be determined using Eqs. (24), (27), and (28).

Observe that two lateral displacements (i.e., Δ_x and Δ_y) are needed to completely characterize the phase-center location, and for this another three sets of constant $\phi + 90$-deg-value radiation-pattern phase measurements towards three directions [i.e., Φ_1, Φ_2, and Φ_3, towards $(\theta_1, \phi + 90 \text{ deg})$, $(\theta_2, \phi + 90 \text{ deg})$, and $(\theta_3, \phi + 90 \text{ deg})$, respectively] are needed. This new set of measurements will also yield C and Δ_z values. However, because of the variation of the radiation pattern with ϕ, these two new values will in general be different than the previously determined two values. How to handle this, as well as other details that stem from the practical application of the above equations, is better demonstrated through an example. This is done in the next section.

III. Application Example

Figures 3 and 4 depict the far-zone co-polarized radiation patterns of a typical linearly polarized corrugated horn (according to Ludwig's third polarization definition). These particular patterns correspond to the CloudSat spacecraft [1] test horn, shown in Fig. 5. The $\phi = 0$ deg, $\phi = 45$ deg, and $\phi = 90$ deg planes

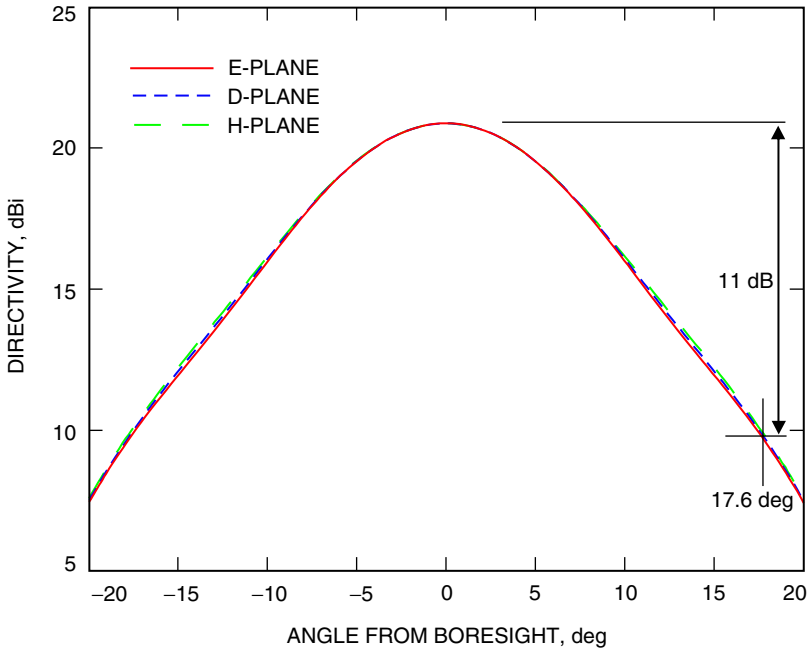

Fig. 3. CloudSat corrugated test horn co-polarized far-zone radiation-pattern amplitude at 94.05 GHz.

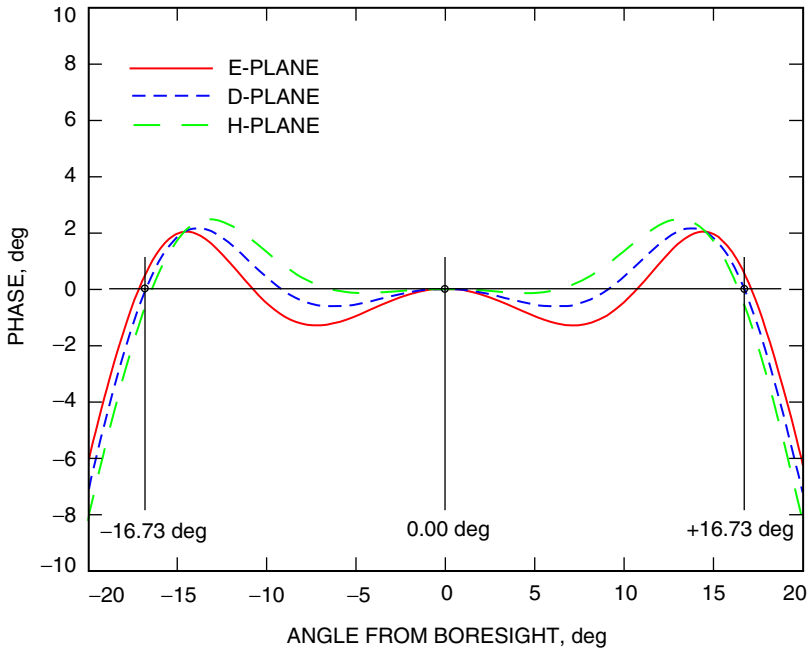

Fig. 4. CloudSat corrugated test horn co-polarized far-zone radiation-pattern phase at 94.05 GHz.

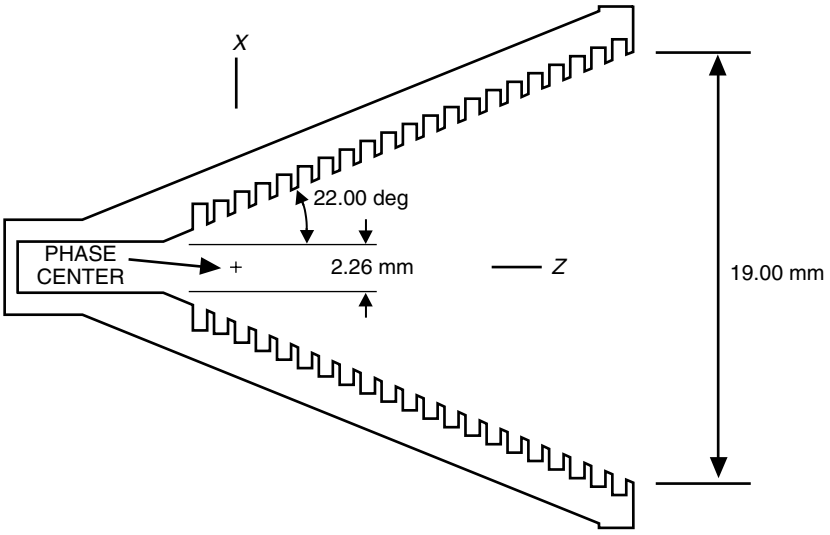

Fig. 5. CloudSat corrugated test horn.

correspond to the E-, D-, and H-planes, respectively. These patterns were computed rotating the horn about the phase-center point depicted in Fig. 5, at a frequency of 94.05 GHz ($\lambda_0 = 3.1876$ mm). Observe that, since the purpose of this horn is to illuminate a reflector system, this phase-center location produces essentially a constant phase (within about ± 3 deg) over a pattern amplitude range of 11 dB (angular region with -17.6 deg $< \theta < +17.6$ deg). In other words, the phase center is here defined as the point that minimizes that radiation pattern phase variation over the angular region with -17.6 deg $< \theta < +17.6$ deg. From Fig. 4 it can be seen that, at each constant ϕ plane, the phase is equal to zero at five points. Imposing the condition that the phase be zero at $\theta = -16.73$ deg, 0 deg, and $+16.73$ deg on the D-plane (i.e., plane with $\phi = 45$ deg) then locates the phase center as shown in Fig. 5 and produces the plot shown in Fig. 4.

Consider now the phase patterns depicted in Fig. 6. These radiation patterns were computed rotating the horn about a point with $\Delta_x = +127$ μm, $\Delta_y = +63.5$ μm, and $\Delta_z = +635$ μm (see Figs. 1 and 2). To demonstrate the application of the previously derived phase-center location equations, these values of Δ_x, Δ_y, and Δ_z are retrieved below by applying the formulas derived in the previous section to the patterns depicted in Fig. 6.

From the points marked in the E-plane pattern of Fig. 6, one obtains

$$\Phi_{E1} = +65.12 \text{ deg at } \theta_1 = -16.73 \text{ deg}$$

$$\Phi_{E2} = +71.72 \text{ deg at } \theta_2 = 0.00 \text{ deg}$$

$$\Phi_{E3} = +73.38 \text{ deg at } \theta_3 = +16.73 \text{ deg}$$

which yields, after substituting in Eqs. (27), (28), and (24), the parameters of the E-plane phase center:

$$\Delta_{Ez} = +516.69 \ \mu\text{m}$$

$$\Delta_{Ex} = +127.04 \ \mu\text{m}$$

$$C_E = +13.37 \text{ deg}$$

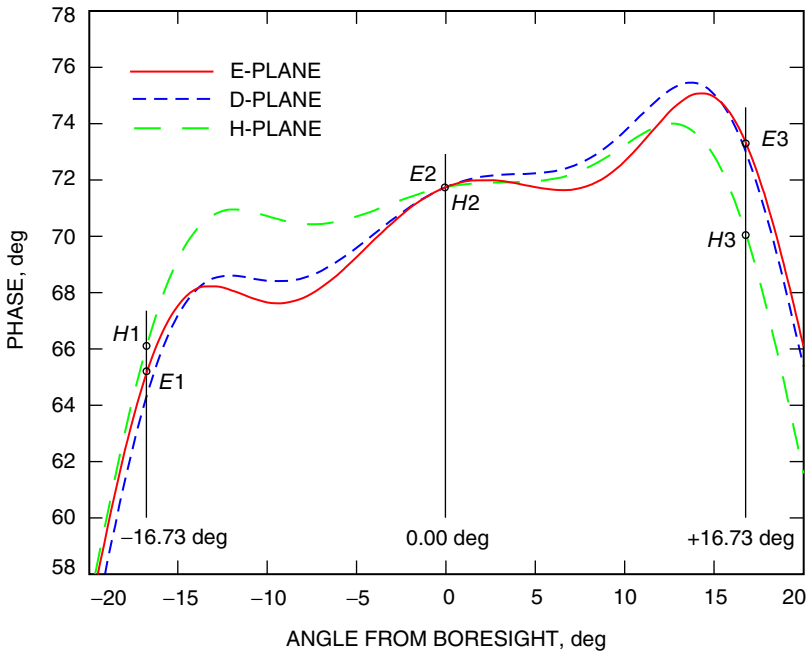

Fig. 6. CloudSat corrugated test horn co-polarized far-zone radiation-pattern phase for Δ_x = +127 μm, Δ_y = +63.5 μm, and Δ_z = +635 μm at 94.05 GHz.

Similarly, from the H-plane pattern of Fig. 6, one obtains

$$\Phi_{H1} = +66.07 \text{ deg at } \theta_1 = -16.73 \text{ deg}$$

$$\Phi_{H2} = +71.72 \text{ deg at } \theta_2 = 0.00 \text{ deg}$$

$$\Phi_{H3} = +70.20 \text{ deg at } \theta_3 = +16.73 \text{ deg}$$

and hence the parameters of the H-plane phase-center location are

$$\Delta_{Hz} = +749.93 \ \mu\text{m}$$

$$\Delta_{Hy} = +63.52 \ \mu\text{m}$$

$$C_H = -12.98 \text{ deg}$$

As expected from Fig. 4, the E- and H-plane phase centers differ slightly (i.e., $\Delta_{Ez} \neq \Delta_{Hz}$ and $C_E \neq C_H$). The best phase-center location is then a compromise between the two phase centers. Taking the average of the above two Δ_z and C values yields the phase-center location as

$$\Delta_x = +127.0 \ \mu\text{m}$$

$$\Delta_y = +63.5 \ \mu\text{m}$$

$$\Delta_z = +633.3 \ \mu\text{m}$$

$$C = +0.2 \text{ deg}$$

which compares very well with the expected values of $\Delta_x = +127$ μm, $\Delta_y = +63.5$ μm, $\Delta_z = +635$ μm, and $C = 0$ deg.

IV. Conclusion

An expression for the phase error inflicted on the measured radiation pattern of an improperly aligned antenna has been derived. From this result a procedure for determining the antenna phase-center location has been presented. The procedure usage and accuracy is successfully demonstrated through an example using a computed corrugated horn far-zone radiation pattern.

Acknowledgments

The author is grateful for clarifying conversations about this to topic with L. Amaro and O. Quintero.

Reference

[1] S. Spitz, A. Prata, J. Harrell, R. Perez, and W. Veruttipong "A 94 GHz Spaceborne Cloud Profiling Radar Antenna System," 2001 IEEE Aerospace Conference, Big Sky, Montana, March 10–17, 2001.